Master of Science
Computational Mechanics

Year 2017/2018

Master Thesis

submitted by

Arada JAMNONGPIPATKUL

TITLE

Massively parallel computations for micro-mechanical modelling of fiber suspensions

Advised by: Luisa Rocha da SILVA
Location: High Performance Computing Instituite, ECN

Abstract

Composite materials, through its combine lightness and strength, contribute to the weight saving of structural parts. However, complexity of their microstructure requires massively parallel methods and high performance computing to establish realistic modelling of real samples, in particular for fiber-reinforced polymers. This study is the beginning step in using the existing tool, CimLib, to model microstructures of fiber and matrix and evaluate local stresses around the fiber. A simple 3D configuration is used to validate the implementation of nonlinear constitutive law.

Keywords: elastic-plastic matrix, immersed volume method, level set method, stress localization

Contents

List of Figures

Chapter 1: Introduction

The use of composite material has gained popularity in many industries thanks to its enhanced mechanical properties and weight reduction when compared to traditional materials. It is a result of combining two or more constituent materials with significantly different material properties to produce a material with certain desired properties while the individual components remain distinguishable within the composite as they do not dissolve or blend into each other. It allows the designer of the product or structure to combine a wide array of materials and choose an optimum combination.

To be able to give the composite unique properties, designers first need to understand the function of each constituent material. Individual materials combined in the composite can be categorized into two types, matrix and reinforcement. The primary functions of the matrix material are to transfer stresses between the reinforcements, maintain relative position of the reinforcements and protect them from mechanical and/or environmental damages while the reinforcement is the main source of strength and contributes its properties to enhance matrix properties. Typical engineered composite materials are, for example, concrete, plywood, fiber-reinforced polymer, ceramic matrix composite and metal matrix composite.

It is of fundamental importance to determine the mechanical properties of the composite. However, macroscopic properties of the composite do not depend only on the properties of the constituents but also on their underlying microscopic structure such as the relative amount of each constituent, fiber shape, size, orientation and distribution. Predicting mechanical behavior of the composite requires the knowledge of the relationship between the microstructure and the macroscopic response. This can be achieved by the development of micromechanical models.

Micromechanics of materials is the analysis of heterogeneous materials on the level of the individual constituents to study the mechanisms operating at the microstructural scale. Since most composite materials show a statistical rather than a deterministic arrangement of the constituents, the concept of representative volume element (RVE) is introduced to be used with methods in micromechanics. It is based on the idea that the microstructure of composite material can be described by a unit cell that is periodically repeated. Therefore, a single repeating volume element is studied. The so-called representative volume element (RVE) is a representation of the heterogeneous material. It should be the smallest volume to determine material properties at the macroscopic scale but large enough to statistically represent the heterogeneities of the composites at the microscopic scale.

To determine effective macroscopic properties such as the elastic tensor of a composite material, a task known as homogenization is performed. Homogenization relies on an asymptotic expansion of the governing equations.

Another key point of micromechanics of materials is to evaluate stress and strain locally in each constituent for given load states, material properties and microstructures. This offers a valuable insight into the effective properties of the composite. For example, the efficiency of stress transfer from matrix to fiber is of fundamental importance in determining the mechanical properties of fiber-reinforced composite materials. The stress transfers depend on the micro-

mechanical characteristics of fiber-matrix interfaces.

Fiber-matrix interface is considered one of the weakest link in the load path. It is crucial to understand the mechanism along fiber-matrix interface in the composite as most failures in fiber-reinforced composites such as debonding, fiber pullout and matrix cracking occur in or near this region. In general, failure mechanism starts from the matrix debonding from the fiber ends at an early stage of loading. This can cause localized plastic deformation but not necessarily lead to other types of damage. Stress concentration from the debonded fiber end can induce matrix cracking and debonding at fiber-matrix interface. As the load increases, these cracks propagate and combine until material fails. The interaction between interface debonding and matrix micro-cracking often makes the development and verification of the micro-damage model complicated. Analysis and simulation of these micro-damage mechanisms can done only through the development of micromechanical models. Ability to understand and describe material damage and failure is important as these micro-damage mechanisms successively impact the mechanical properties of the composite.

1.1 Objectives

In this study, the focus will be on fiber-reinforced polymer. In fiber-reinforced polymer, fibers as the reinforcement are usually glass, carbon, aramid, or basalt while polymer as the matrix can be epoxy, vinyl ester, or polyester. For this type of composite, fibers are specifically used to enhance strength and elasticity of the polymer.

The study is devoted to the validation of the implementation of nonlinear constitutive law in CimLib, the C++ parallel finite element library. A simple 3D configuration is used to illustrate the ability of the framework to deal with 3D microstructures. Micromechanical analyses of unidirectional fiber-reinforced polymer was performed to evaluate stress fields at the fiber-matrix interface.

This report is organized as follows. Chapter 2 presents bibliography. Chapter 3 presents the numerical framework implemented in CimLib. Chapter 4 presents unit cell modeling used in the simulations. Numerical results are presented in chapter 5. Lastly, conclusion is in Chapter 6.

Chapter2: Bibliography

There has been an ongoing effort to develop a realistic model to predict mechanical properties of composite materials.

2.1 Effective property

Extensive models have been developed to predict the effective elastic constants of composite materials. In the beginning, analytical modeling is the common approach with a single fiber, whisker, or particle of simple geometry in a unit cell model. These analytical models include the self-consistent model by Eshelby [1], the Mori-Tanaka model [2] and Halpin-Tsai estimation [3] among others. More recently, Torquato [4] obtained more accurate expressions for the bulk and shear moduli of the isotropic composite by truncating after third-order terms an exact series of expansion being explicitly given as a function of certain statistical correlation parameters which provide information about the phase arrangement.

However, analytical models are limited to capture the real stress-strain relation in the composite. In recent decades, finite element analysis has become an alternative widely employed to predict the effective mechanical properties of composite materials with the implementation of representative volume element (RVE) concept as a common practice. A classical problem is the determination of effective elastic properties of a composite material made up of a statistically isotropic random distribution of isotropic and elastic spherical inclusions embedded in a continuous, isotropic and elastic matrix.

Segurado and Llorca [5] computed elastic constants for 3-D cubic unit cells containing non-overlapping identical spheres randomly distributed in a continuous and isotropic elastic matrix through the finite element analysis to assess the accuracy and range of applicability of 3 analytical models: Mori-Tanaka mean-field analysis, Generalized self-consistent method and Torquato's third-order approximation. They investigated 3 types of materials: rigid spheres in an elastic matrix, spherical voids in an elastic matrix and glass spheres in an epoxy resin. The simulations were performed within the framework of the small displacements theory and the materials were assumed to behave as linear, elastic and isotropic solids. They found that Torquato's third-order approximation tended to provide the best approximation to the numerical results and the Mori-Tanaka method the poorest. The maximum differences between the numerical results and the analytical models were found in the case with rigid spheres while the minimum differences were found in the case with spherical voids.

Liu et al. [6] compared effective elastic constants of discontinuous fiber reinforced composites from FEA using their developed RVE-ESE model with those from Digimat, a commercial software based on Eshelby's single inclusion solution and Mori-Tanaka model. They found that the result differences may attribute to the fact that their developed RVE-ESE model accounts for the effects of fiber interactions more realistically, resulting in a more accurate prediction of the stress-strain states within the composites comparing to the analytical models adopted in Digimat

Segurado et al. [7] investigated the effect of the reinforcement clustering on the mechanical properties of composites. The study was done within the framework of the small displacements theory with elastic and isotropic spherical reinforcements and an isotropic elasto-plastic matrix. They found that the influence of reinforcement clustering on the macroscopic behavior was weak. Average magnitude of stresses and strains were not influenced by the clustering. However, the local values of the maximum principal stress in the spheres and, therefore, the fraction of broken spheres increased with the degree of clustering. The presence of clustering has negative effects on the onset of damage and thus on the overall mechanical properties.

Tian et al. [8] found that bulk and shear modulus of composites increase while the Poisson's ratios decrease with the increasing fiber volume fraction for the composites with spatially randomly distributed short fibers under the assumption that the fibers and matrix are both linear isotropic elastic and that they are perfectly bonded. Bulk and shear modulus is validated against those obtained from the Halpin-Tsai estimation. The error between the Halpin-Tsai estimation and the numerical analysis is found to be less than 4.5%.

2.2 Micro-damage mechanisms

It can be seen that progress has been made significantly to explain the relationship between composite microstructures and elastic properties. However, accurate tools to analyze and simulate micro-damage mechanisms are still absent due to the complexity of micro-damage processes that have not been fully understood.

Huang and Talreja [9] investigated micro-cracking mechanism in short fiber reinforced polymer composites considering strongly bonded fiber-matrix interface with elastic fibers and a ductile matrix. Under this circumstance, interface debonding can be suppressed and matrix micro-cracking becomes the governing mechanism. Rice-Tracey ductile fracture model was used to predict crack initiation and propagation in the matrix in the framework of the local approach to fracture. It was first applied to the case of matrix cracking from the broken fiber end in a fiber fragmentation test of a single-fiber reinforced composite. The model successfully predicted conical crack path including crack initiation angle and kink formation comparing to those measured in the fragmentation test. The model was then applied to the case of micro-cracking in an aligned short fiber composite. The often-observed fiber-avoidance cracking mode in short fiber composites can be predicted by the model.

Jiang and Gao [10] explored how micro-damage mechanisms like debonding and interfacial slipping can affect the overall composite strength. They used shear-lag theory and special frictional contact element method to analyze stress transfer from matrix to fiber in metal-matrix composites as the efficiency of stress transfer is of fundamental importance in determining mechanical properties of composite materials. They considered a single short fiber in an elastic matrix and verified that the end interface between short fiber and matrix is easy to debond during loading process. Therefore, the model of a perfectly bonded fiber-matrix interface cannot reflect the real interfacial condition when the load is applied. After fiber-matrix interfacial debonding occurs at the fiber end, the stress transfer from matrix to fiber then only depends on the shear stress on axial interface.

2.3 Stress localization

After all, to be able to understand the influence of microstructural features on the initiation and evolution of the micro-damages, understanding the evolution of local stresses is of fundamental importance. The pioneering work of Eshelby [1]studied the deformation of an isolated ellipsoidal inclusion in an infinite matrix submitted to remote homogeneous loading in the case where both the inclusion and the matrix are isotropic and linearly elastic. He gave the exact displacement field in an explicit form inside and outside the inclusion. The derivation shows that the strain is homogeneous within the inclusion. Tandon and Weng [11] studied elastic stress and energy distribution in and around spheroidal inclusions and voids at finite concentration. They developed a close-form solution based on Eshelby's solution of an ellipsoidal inclusion and Mori-Tanaka's concept of average stress in the matrix.

Since the matrix material typically undergoes plastic deformation before damage occurs, several studies of the stress and strain state at the interface between a elastic reinforcement and a plastically deforming matrix have been performed.

Orr and Brown [12] used finite differences and successive over-relaxation and presented elasto-plastic stress and strain fields on the matrix-inclusion interface. They considered plain strain conditions, rigid cylindrical inclusion and the matrix obeying the Mises yield criterion and its associated flow rule.

Wilner [13] studied the deformation of an isolated elastic spherical particle embedded in an elastic-plastic infinite matrix material subject to an axisymmetrical load. He found that at large loads the stress concentration factor at the particle-matrix interface asymptotes to a constant value which depends strongly on the strain hardening exponent and the stress triaxiality.

Lee and Mear [14] evaluated local stress concentration factors at the particle-matrix interface and within the particle using a Ritz procedure. A single isolated linearly elastic, prolate spheroidal particle embedded in a plastically deforming matrix was considered to also investigate the effect of particle shape. They found that the particle shape has a strong effect on the stress concentration factors with the degree of influence also depending on material properties and triaxiality of the remote loading.

Briottet et al. [15] investigated the strain rate in an inclusion embedded in a matrix undergoing large strains. Since analytical solution for the localization factor cannot be derived when the matrix is not linear, they proposed approximate analytical equations to find the localization factor from strain rate sensitivity parameter as well as from inclusion hardness and aspect ratios. The analytical approximation is found to be in good agreement with those obtained from the variational approach.

Ahmadi and Aghdam [16] used a truly meshless method based on the meshless local Petrov-Galerkin method to study elastic-plastic behavior of heterogeneous solid materials. They assumed the fully bonded fiber-matrix interface condition and imposed the continuity of displacement and reciprocity of traction at the interface. Micro-stresses and micro-strains in the unidirectional Boron-Aluminium metal matrix composite were compared with the predictions from finite element method and found to be in excellent agreement.

Most of the studies have been performed for the unidirectional composites under transverse tension or compression, and only a few concerned the mechanical behavior of composites under transverse shear load. Understanding of micro-mechanical response of composite under trans-

verse shear load is also important to the overall characterization of composites for the design application of composite materials.

Schmid and Podladchikov [17] used Muskhelishvili's method to derive closed-form analytical solutions for an isolated deformable elliptical inclusion in a matrix subject to general shear far-field flow in 2-D viscous as well as elastic problems. Muskhelishvili's method provides analytical formula well-known for calculating stress concentration around holes and recesses in engineering structures and machines. The basis of Muskhelishvili's method is that the equation describing 2-D plane stress or plane strain problem has a general solution that can be expressed in terms of two functions in complex coordinate system. They demonstrated how stresses, velocities and other parameters can be evaluated from these two complex functions.

Most analytical and numerical models assume that the bond between the reinforcement and matrix is perfect and can be modeled using the continuity of tractions and displacements across the discrete interface. However, there are thin layers between the reinforcement and the matrix. These so-called interphases can be formed unintentionally due to the chemical reaction between matrix and reinforcement material or intentionally due to the use protective coatings on the reinforcements during manufacturing to ensure good adhesion between reinforcement and matrix material. These interphases can significantly affect the mechanical properties and failure mechanisms of composite material.

Pak et al. [18] studied a coated circular inclusion embedded in an infinite matrix in the framework of two-dimensional isotropic linear elasticity. A closed-form solution is obtained using Muskhelishvili's complex potential method for the case of far-field uniaxial tension.

Voros and Pukanszky [19] accounted for a soft interlayer with changing properties around an inclusion embedded into an infinite matrix to predict the effect of the soft interlayer on stress distribution. They found that a soft interphase changes stress distribution and decreases stress concentration.

Lauke and Schuller [20] studied stress field around a particle under uniaxial load. They considered a coated particle embedded within a cylindrical rod. They found that stress concentration strongly depends on the ratio between the elastic modulus of the matrix and the interphase and on the Poisson's ratio of the interphase.

Sun et al. [21] performed a multi-scale computational analysis based on representative volume element modeling and molecular dynamics simulations to investigate the microscopic failure mechanisms of unidirectional carbon fiber-reinforced polymer composites. By adding the interphase region, they were able to capture stress-strain behavior compared to the experimental data.

2.4 Immersed volume method

Immersed volume method implemented in CimLib has been applied in many applications. Silva et al. [22] proposed a numerical approach to determine permeability at the mesoscopic and microscopic scale in liquid composite moulding processes. The interface between fibers or yarns and fluid was captured through the level set approach. Hachem et al. [23] used the immersed volume approach for thermal coupling between fluids and solids for heating high-alloy steel inside industrial furnaces. Level set technique was used to model fixed but complex boundaries. Roux et al. [24] used the level set framework coupled with an anisotropic remeshing

technique to track interfaces of matrix-inclusions and matrix-voids at large plastic strain. They were able to present void growth process for a 2D real complex microstructure and for a simple 3D microstructure. Munoz et al. [25] presented a numerical method to simulate fluid-elastic solid interaction with surface tension. Level set method was used to capture the interface between the solid bodies and the incompressible surrounding fluid.

Chapter 3: Numerical Framework

In this study, the simulations were carried out using the finite element library CimLib, a fully parallel C++ scientific code developed mainly at CEMEF at MINES ParisTech [26]. CimLib is capable of solving a single set of equations for the whole computational domain and treating different subdomains as a single geometrical domain with variable material properties. Stabilized finite element method and a level set approach are used. Theoretical basis implemented in CimLib is presented in this chapter.

3.1 Constitutive equations

The unit cell considered in this study contains two different materials, fiber and matrix. In this study, fiber is assumed to be purely elastic while matrix is considered as an elasto-plastic solid. The definition of the constitutive model for both material is described in this section.

Hooke's law is used to model elasticity in fiber. The elastic behavior is defined by a linear relationship between the stress tensor $\boldsymbol{\sigma}$ and the elastic strain $\boldsymbol{\varepsilon}^e$

$$\boldsymbol{\sigma} = \mathbf{D}^e : \boldsymbol{\varepsilon}^e \tag{3.1}$$

where $\mathbf{D}^e$ is the standard isotropic elasticity fourth-order tensor.

The matrix is taken to be elastic-plastic obeying the von Mises yield criterion. The elastic-plastic constitutive law is based on the decomposition of the total strain increment $\dot{\boldsymbol{\varepsilon}}$ in two parts

$$\dot{\boldsymbol{\varepsilon}} = (\dot{\boldsymbol{\varepsilon}}^e + \dot{\boldsymbol{\varepsilon}}^p) \tag{3.2}$$

where $\dot{\boldsymbol{\varepsilon}}^e$ is the elastic part and $\dot{\boldsymbol{\varepsilon}}^p$ is the plastic part.

Therefore, the elastic behavior of the fiber and the initial elastic behavior of the matrix must be written as

$$\dot{\boldsymbol{\sigma}} = \lambda tr(\dot{\boldsymbol{\varepsilon}}^e) I_d + 2\mu \dot{\boldsymbol{\varepsilon}}^e \tag{3.3}$$

where λ and μ are the Lamé coefficients and I_d is the identity matrix.

The elastic strain rate tensor $\dot{\boldsymbol{\varepsilon}}^{\boldsymbol{e}}$ is defined based on the velocity field $\mathbf{v}$.

$$\dot{\boldsymbol{\varepsilon}}^e = \frac{1}{2}(\nabla \mathbf{v} - \nabla^T \mathbf{v}) \tag{3.4}$$

The plastic part of the strain rate tensor is computed using the following flow rule

$$\mathbf{S} = \frac{2}{3}\boldsymbol{\sigma}_0(\bar{\varepsilon})\frac{\dot{\boldsymbol{\varepsilon}}^p}{\dot{\bar{\varepsilon}}} \tag{3.5}$$

where $\mathbf{S}$ is the deviatoric part of the stress tensor, $\boldsymbol{\sigma}_0$ is the flow stress, $\bar{\varepsilon}$ is the equivalent strain and $\dot{\bar{\varepsilon}}$ is the equivalent strain rate.

The flow stress is governed by a hardening law of the following form

$$\boldsymbol{\sigma}_0(\bar{\varepsilon}) = \boldsymbol{\sigma}_y + K\bar{\varepsilon}^n \tag{3.6}$$

where K is the plastic consistency, $\boldsymbol{\sigma}_y$ is the yield stress, and n is the hardening exponent.

3.2 Stabilized finite element method

In CimLib, a mixed finite element velocity-pressure formulation with the mini-element (P1+/P1) is used to solve the elastic-plastic problem. The nonlinearity due to the plastic behavior of the matrix is solved implicitly using Newton-Raphson algorithm. In this section, mixed velocity/-pressure formulation is established for the global coupled mechanical problem and discretized using a continuous linear approximation in both velocity and pressure.

3.2.1 Finite element formulation

Mixed velocity-pressure formulation is derived based on the separation of Cauchy stress tensor into its deviatoric and volumetric part. The field equations governing the problem are the equilibrium equation and the continuity equation.

$$\begin{aligned} \mathrm{div}(\mathbf{S}) - \nabla p = 0 \quad \text{in } \Omega, \\ \mathrm{tr}\dot{\boldsymbol{\varepsilon}} + \frac{\dot{p}}{\kappa} = 0 \quad \text{in } \Omega \end{aligned} \tag{3.7}$$

where $\mathbf{S}$ and p are the deviatoric and volumetric components of the stress tensor $\boldsymbol{\sigma}$ and κ is the bulk modulus of material.

The formulation of the finite element problem is obtained by multiplying the equation set (3.7) by an appropriate test functions, applying the divergence theorem and integrating over the domain of interest with appropriate boundary conditions. The weak form reads

$$\begin{aligned} \int_\Omega \mathbf{S}(\mathbf{v}) : \dot{\boldsymbol{\varepsilon}}(\mathbf{v}^*)\mathrm{d}\Omega - \int_\Omega p\ \mathrm{tr}\big(\dot{\boldsymbol{\varepsilon}}(\mathbf{v}^*)\big)\mathrm{d}\Omega - \int_{\partial\Omega} \mathbf{T}\cdot\mathbf{v}^*\mathrm{d}S = 0 \quad \forall \mathbf{v}^*, \\ \int_\Omega p^*\left(\mathrm{tr}\dot{\boldsymbol{\varepsilon}}(\mathbf{v}^*) + \frac{\dot{p}}{\kappa}\right)\mathrm{d}\Omega = 0 \quad \forall p^* \end{aligned} \tag{3.8}$$

where $\mathbf{v}^*$ is the virtual velocity field and p^* is the virtual pressure field. The equation set (3.8) holds for any virtual velocity $\mathbf{v}^*$ and pressure p^* fields defined over the configuration at time t

3.2.2 Space and time discretization

The finite element spatial discretization of mixed formulation (3.8) is done using the mini-element (P1+/P1). This mini-element has linear continuous interpolation of both pressure and velocity and a bubble enrichment of the velocity added at its center. Adding a velocity node at the center of the element can be seen as a decomposition into four subtetrahedra. It enriches the velocity space with a space of bubbles using a polynomial function of order one with a value equal to unity at the center of the element and vanishing at its boundary. This bubble function is necessary for the satisfaction of the LBB stability condition. This first-order element works well with unstructured meshes, iterative methods and parallel computing. The illustration of the mini-element for 3D problem is shown in Figure 3.1.

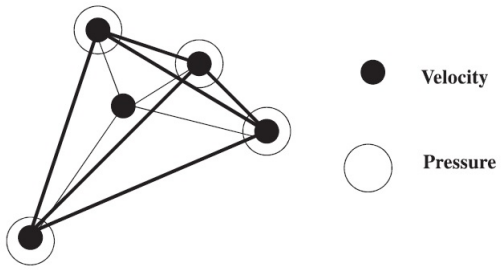

Figure 3.1: Mini element (P1+/P1)

After discretization and using the bubble function properties, the algebraic problem arising from the finite element formulation are assembled and can be written in the matrix form:

$$\begin{bmatrix} A_{vv} & A_{vb} & A_{vp} \\ A_{vb}^T & A_{bb} & A_{bp} \\ A_{vp}^T & A_{bp}^T & 0 \end{bmatrix} \begin{bmatrix} v_h \\ b_h \\ p_h \end{bmatrix} = \begin{bmatrix} 0 \\ 0 \\ 0 \end{bmatrix} \tag{3.9}$$

Bubble condensation provides the system with only the main variables v_h and p_h in the following form

$$\begin{bmatrix} A_{vv} - A_{vb}A_{bb}^{-1}A_{vb}^T & A_{vp} - A_{vb}A_{bb}^{-1}A_{bp} \\ A_{vp}^T - A_{bp}^T A_{bb}^{-1}A_{vb}^T & -A_{bp}^T A_{bb}^{-1}A_{bp} \end{bmatrix} \begin{bmatrix} v_h \\ p_h \end{bmatrix} = \begin{bmatrix} 0 \\ 0 \end{bmatrix} \tag{3.10}$$

where

$$\begin{bmatrix} A_{vv} - A_{vb}A_{bb}^{-1}A_{vb}^T & A_{vp} - A_{vb}A_{bb}^{-1}A_{bp} \\ A_{vp}^T - A_{bp}^T A_{bb}^{-1}A_{vb}^T & -A_{bp}^T A_{bb}^{-1}A_{bp} \end{bmatrix}$$

is the stabilization matrix. The microstructure is subjected to small strain increments. Therefore, during each time interval, the system (3.10) is a global nonlinear algebraic system of

equations for the velocity field and the pressure field due to the elastic-plastic behavior law. Newton-Raphson algorithm is used to solve iteratively until convergence.

Furthermore, due to the sparsity of the discretized system, the resolution of such system accounts for a significant fraction of the overall simulation time. Conjugate residual method associated with the incomplete LU preconditioner from the Portable Extensive Toolkit for Scientific Computation (PETSc) library is also used in CimLib to obtain the nodal distributions of the velocity and pressure fields.

Though the constitutive relation used in CimLib is a function of pressure and velocity while the mechanical behavior of the solid classically depends on displacement and pressure, the velocity is clearly the derivative of the displacement with respect to time. Once convergence is achieve, the configuration of the body can thus be updated at the end of the time step using an Euler explicit scheme.

$$\mathbf{v} = \frac{\mathbf{u} - \mathbf{u}^{t-\Delta t}}{\Delta t} \tag{3.11}$$

where $\mathbf{u}$ and $\mathbf{v}$ are the displacement and velocity fields at the current time t, $\mathbf{u}^{t-\Delta t}$ is the displacement field at time $t - \Delta t$, and Δt is the time step. The displacement $\mathbf{u}^{t-\Delta t}$ is known at the current time t.

3.3 Immersed volume method

To perform simulations, the geometry needs to be defined accurately and mechanical properties needs to be assigned for the whole computational domain. The immersed volume method is used in CimLib. This section presents the description of the approach from immersing and defining the fiber using the level set function, appropriately mixing material properties for both domains and applying mesh adaptation in the vicinity of the fiber-matrix interface.

3.3.1 Level set approach

In this study, the computational domain Ω consists of two different phases, Ω_m and Ω_f, representing matrix and fibers in the composite material, respectively. Since computation is performed using a single mesh in CimLib, fiber-matrix interface Γ is thus described implicitly using level set method. In this study, the interface is static and the following statement must be verified.

$$\Omega_m \cup \Omega_f = \Omega \quad \text{and} \quad \Omega_m \cap \Omega_f = \Gamma \tag{3.12}$$

For each node in the computational domain Ω, the level set function ϕ defined as a signed distance function is described by the following conditions

$$\phi(\mathbf{x}) = \begin{cases} -\text{dist}(\mathbf{x}, \Gamma) & \text{if } \mathbf{x} \in \Omega_m \\ \text{dist}(\mathbf{x}, \Gamma) & \text{if } \mathbf{x} \in \Omega_f \\ 0 & \text{if } \mathbf{x} \in \Gamma \end{cases}$$

where dist$(\mathbf{x}, \Gamma)$ is the distance from the node position $\mathbf{x}$ to the closest interface Γ and considered positive if the node is inside the fiber. As a result, Γ is described by the isosurface $\phi(\mathbf{x}) = 0$

Since the interface is not explicitly described by nodes of the mesh but by the level set function, some elements are therefore crossed by the interface and made of two different phases as shown in Figure 3.2.

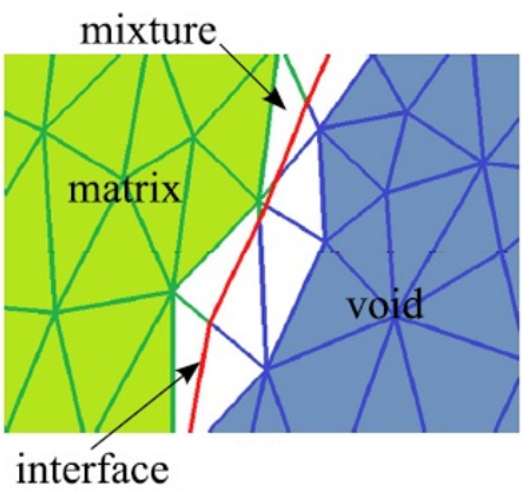

Figure 3.2: Implicit interface [27]

Different mechanical properties within an element are calculated as a function of ϕ by means of mixture law. For instance, the mixed parameter P, such as the elastic constants, is a linear interpolation between the values of parameter P_m in the matrix and P_f in the fiber.

$$P = P_m H(\phi) + P_f(1 - H(\phi)) \tag{3.13}$$

where H is a smoothed Heaviside function given by:

$$H(\phi) = \begin{cases} 1 & \text{if } \phi > e \\ \frac{1}{2}(1 + \frac{\phi}{e}) & \text{if } |\phi| \leq e \\ 0 & \text{if } \phi < -e \end{cases}$$

where e is the thickness of the mixture zone or the so-called interface thickness such that $e = O(h)$ when h is the mesh size in the normal direction of the interface. This mesh size h can be computed from the following expression

$$h_i = \max_{j,l \in K} \nabla\phi \cdot \mathbf{x}^{jl} \tag{3.14}$$

where $\mathbf{x}^{jl} = \mathbf{x}^l - \mathbf{x}^j$ and K is the mesh element.

3.3.2 Mesh adaptation

In CimLib, an isotropic homogeneous mesh is first constructed. As shown in Figure 3.3, this initial mesh is coarse and unstructured and does not necessarily conform to the fiber-matrix interface represented by the blue circle in the figure. To accurately describe the interface, mesh adaptation is performed in a narrow band around the interface resulting in smaller element size in that region.

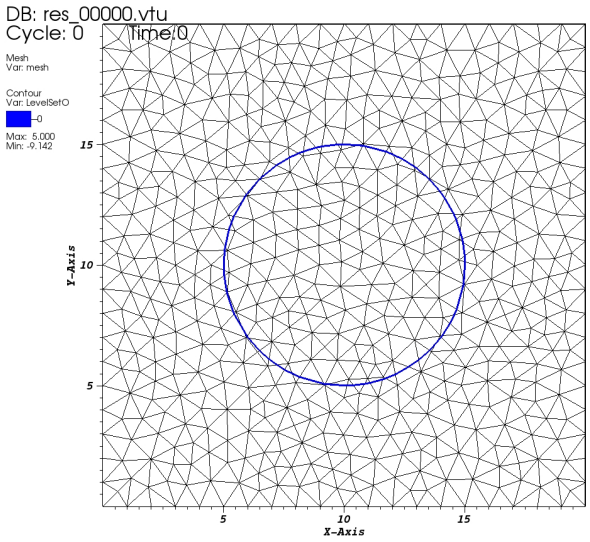

Figure 3.3: Initial mesh

Mesh adaptation is an iterating process consisting of node generation, node deletion and node repositioning. From the initial mesh through several steps, refined elements are added near the interface and, at the same time, some mesh elements far from the interface may be removed until a suitable mesh is obtained. Figure 3.4 illustrates the adaptation at matrix-fiber interface.

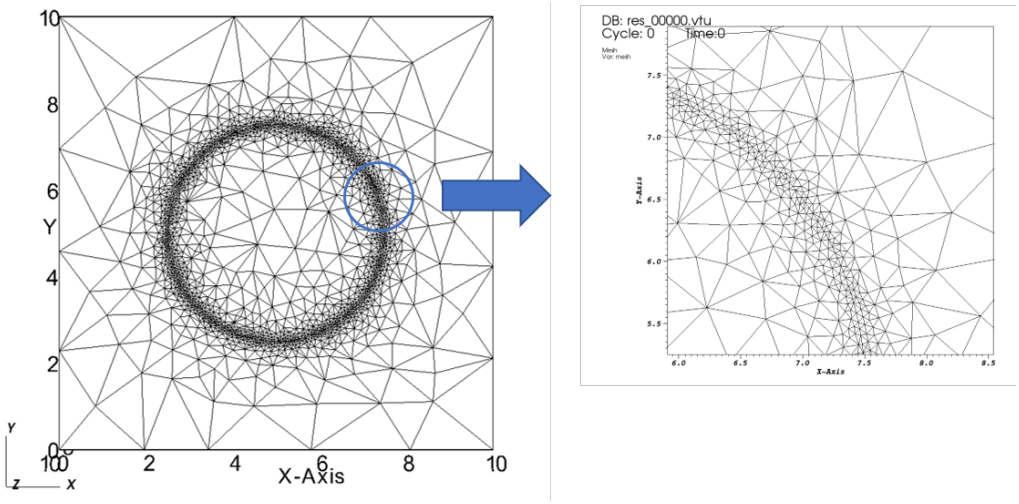

Figure 3.4: An example of isotropic adaptive mesh

In practice, mesh adaptation is performed in a band $\{\mathbf{x} \text{ s.t. } |\phi(\mathbf{x}) \leq e\}$ of thickness $2e$ around the interface. During the adaptation, a default mesh size h_d is imposed far from the interface. Mesh size is reduced as the element is closer to the interface. The element size is computed by linearly interpolating between the minimal value h_Γ at the interface and the default mesh size h_d.

$$h(\mathbf{x}) = \begin{cases} h_d & \text{if } |\phi(x)| > e \\ h_\Gamma + \frac{h_d - h_\Gamma}{e}|\phi(\mathbf{x})| & \text{if } |\phi(x)| \leq e \end{cases} \tag{3.15}$$

Eventually, the mesh becomes locally refined with the sharply defined interface. This strategy allows to save a great number of elements compared to the uniformly refined mesh.

Chapter 4: Unit cell modeling

In this study, the finite element micromechanical models are developed as a cube unit cell based on the unidirectional fiber packing. The fibers are considered as cylinders with a uniform radius distributed within the matrix as shown in Figure 4.1.

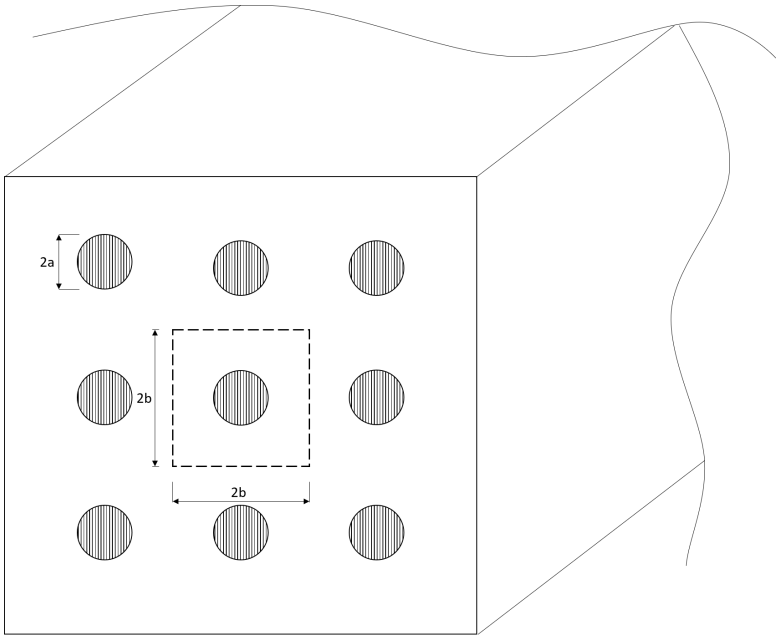

Figure 4.1: Fiber packing with the unit cell indicated

The coordinates system used is shown in Figure 4.2

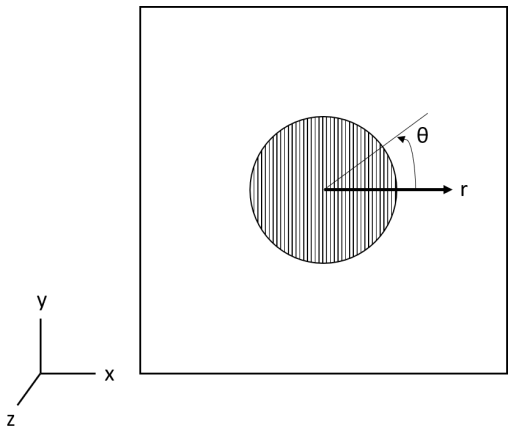

Figure 4.2: Coordinated system used in the analysis

The fiber-reinforced polymer of interest is subjected to uniaxial tensile loading and shear in the transverse direction as shown in Figure 4.3.

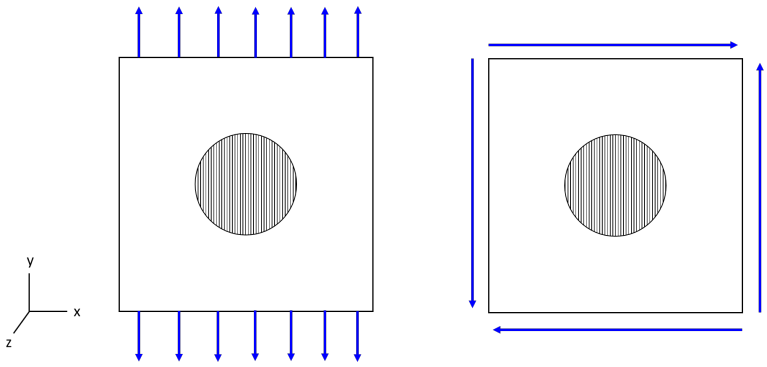

Figure 4.3: Uniaxial tensile and shear loading

However, the implementation in CimLib is velocity oriented. Velocity is thus prescribed on the upper and lower boundaries while the lateral boundaries are subjected to either fixed or free boundary conditions. A cubic finite element model used in the analysis is shown in Figure 4.4

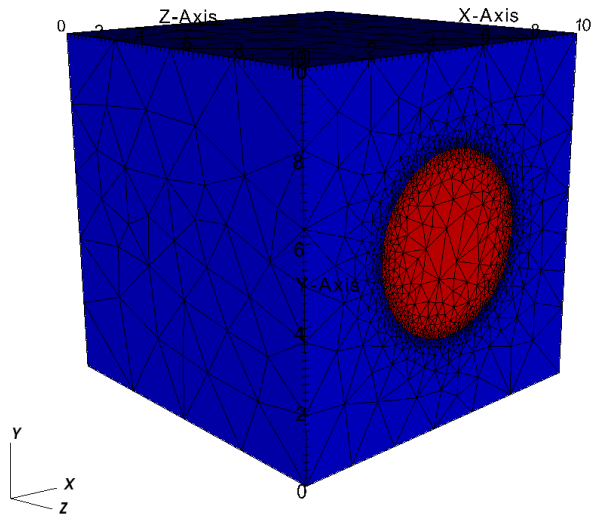

Figure 4.4: Finite element model

In this study, the unidirectional glass epoxy composite with 20% fiber volume fraction is considered. Matrix and fibers are homogeneous and isotropic. Fiber behavior is assumed to be purely elastic while matrix behavior is defined by an elastic-plastic power law as stated in the previous chapter.The stress in which the first yield is seen in the matrix (yield stress) is assumed to be $\sigma_Y = 50$ MPa. Properties used in the simulations: $E_m = 3$ GPa, $E_f = 70$ GPa, $\nu_m = 0.35$, $\nu_f = 0.2$, $K_m = 50$ MPa, $n_m = 2$ where the subscripts m and f correspond to matrix phase and fiber phase, respectively.

Chapter 5: Numerical Results

The results of three-dimensional finite element calculations are presented in this section for a uniform fiber packing embedded in an elastic-plastic matrix. The analysis examines the local fields in the region of fiber-matrix interface under transverse uniaxial tension and shear. All simulations were carried out by using CimLib.

5.1 Plastic zones

The evolution of the plastic zone in the matrix due to the transverse uniaxial tension is shown in Figure 5.1. It can be seen that yielding first starts at some distance from the fiber in the tensile direction as seen in Figure 5.1a and almost simultaneously along the interface at some degrees from the tensile direction as seen in Figure 5.1b. Increase in the prescribed displacement leads to the growth and overlap of two plastic zones and results in an elastic cap as seen in Figure 5.1c. As the load is increased, the elastic cap shrinks while another plastic zone occurs at the side of the unit cell and expands perpendicular to the tensile direction towards the fiber as seen in Figure 5.1d and Figure 5.1e. Again, two plastic zones overlap as seen in Figure 5.1f. The last point to yield is on the interface at $\theta = 0$ as seen in Figure 5.1g and Figure 5.1h.

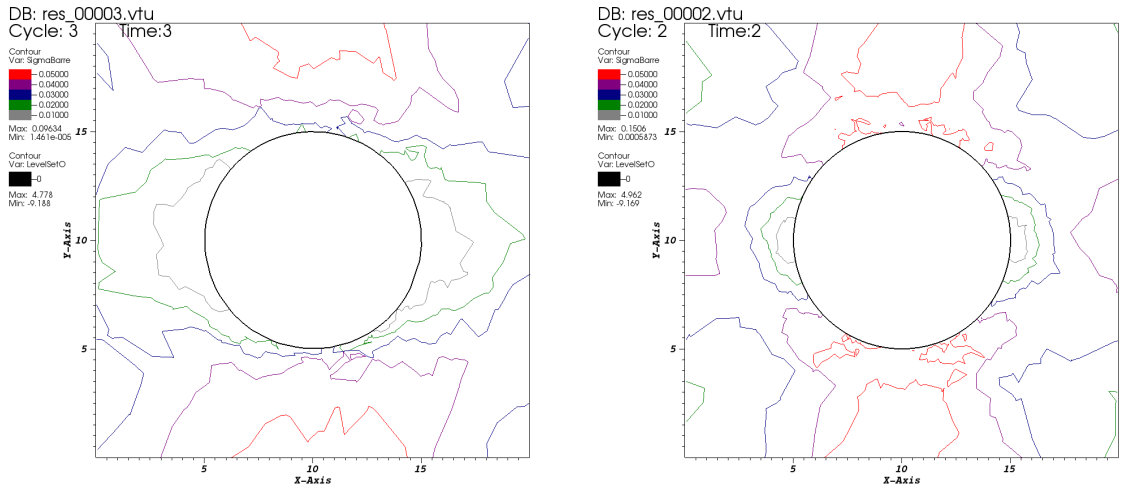

(a) $\varepsilon_y = 0.009$ (b) $\varepsilon_y = 0.010$

Figure 5.1: Plastic zone due to uniaxial tension

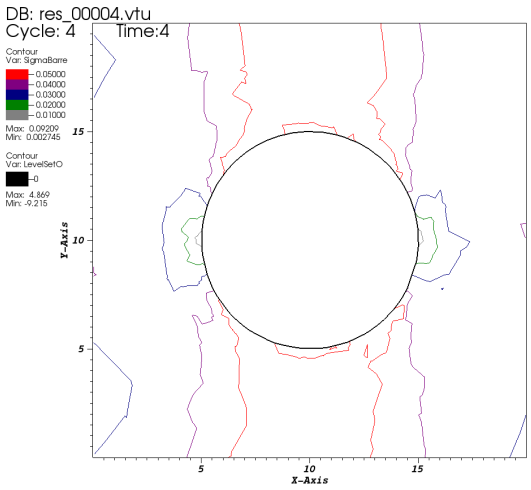

(c) $\varepsilon_y = 0.012$

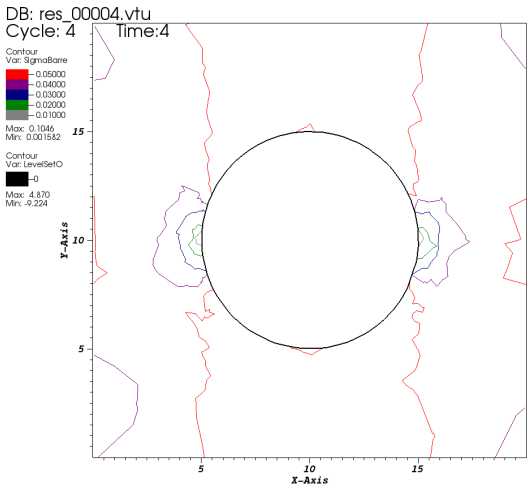

(d) $\varepsilon_y = 0.016$

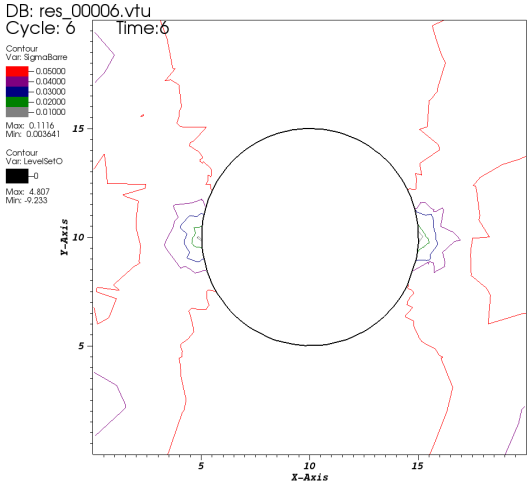

(e) $\varepsilon_y = 0.018$

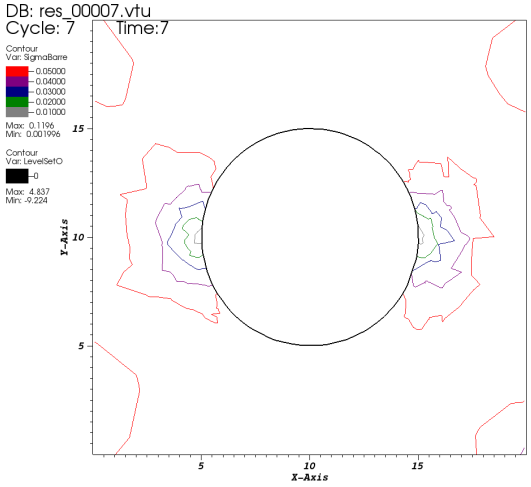

(f) $\varepsilon_y = 0.021$

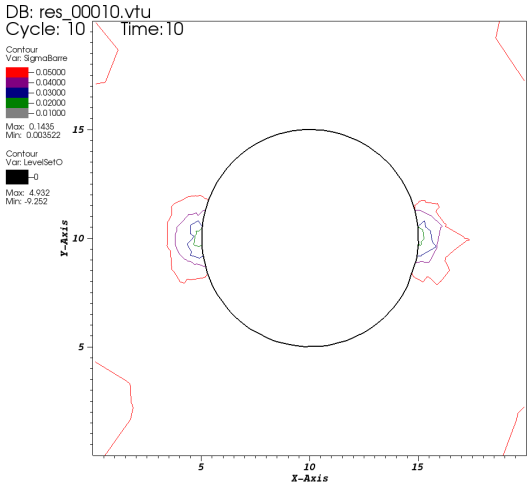

(g) $\varepsilon_y = 0.025$

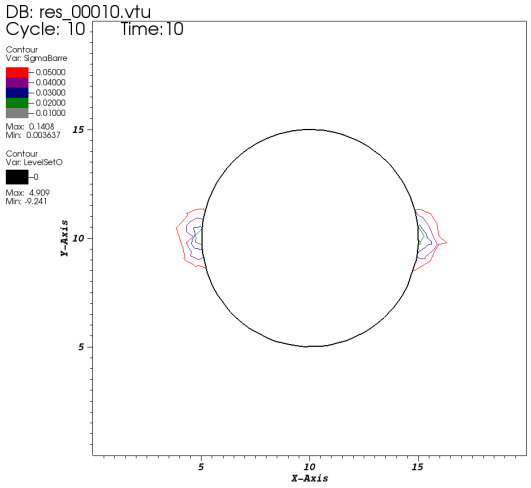

(h) $\varepsilon_y = 0.03$

Figure 5.1: Plastic zone due to uniaxial tension (cont.)

The fact that the stiff fiber deforms less than the surrounding matrix and the displacement continuity is imposed along the fiber-matrix interface can be the reason that the matrix around the fiber remains elastic after the matrix elsewhere has already yielded. For the plastic deformation directly above the fiber, the matrix in that region deforms more than other region to maintain compatibility with the prescribed displacement.

Figure 5.2 shows the comparison of stress contours between the case with elastic matrix and the case with elastic-plastic matrix under the same prescribed displacement. It can be seen that stress increases gradually from $\theta = 0°$ to $\theta = 90°$ when the matrix is elastic while the elastic cap is forming when the matrix is elastic-plastic.

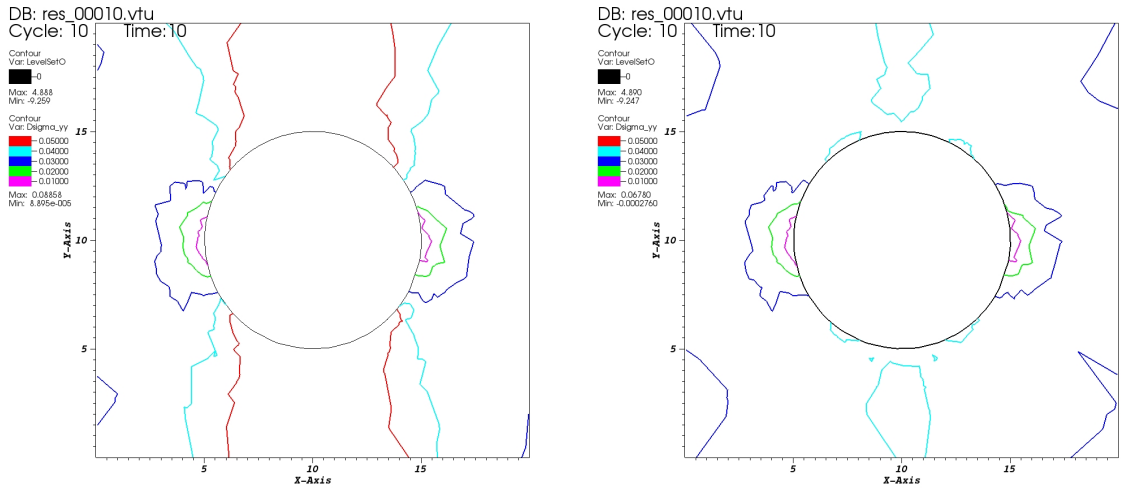

(a) Elastic (b) Elastic-Plastic

Figure 5.2: Effect of plasticity on stress contour

Figure 5.3 shows that most of the plastic deformation lies in shear bands oriented in the direction of maximum macroscopic shear. These shear bands lie in the diagonal direction of the fiber ($\theta = 45°$).

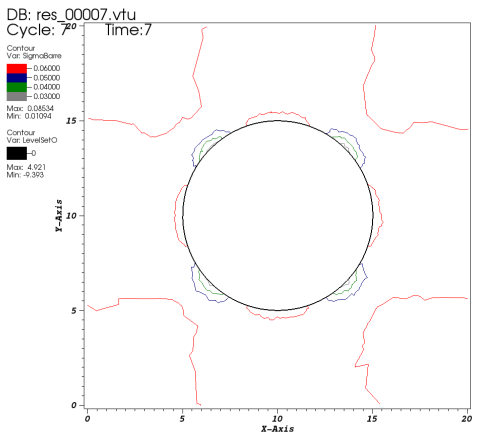

Figure 5.3: Stress contour due to shear load

5.2 Stress distribution around the fiber

Stress distributions around the fiber at the matrix-fiber interface under transverse uniaxial tensile load and shear load are discussed in this section. Results are presented as a function of the angular position from $\theta = 0°$ to $\theta = 90°$ between the equator and the pole. Figure 5.4 compares the stress distributions around the fiber when the fiber is embedded in an elastic matrix and in an elastic-plastic matrix subjected to uniaxial tension.

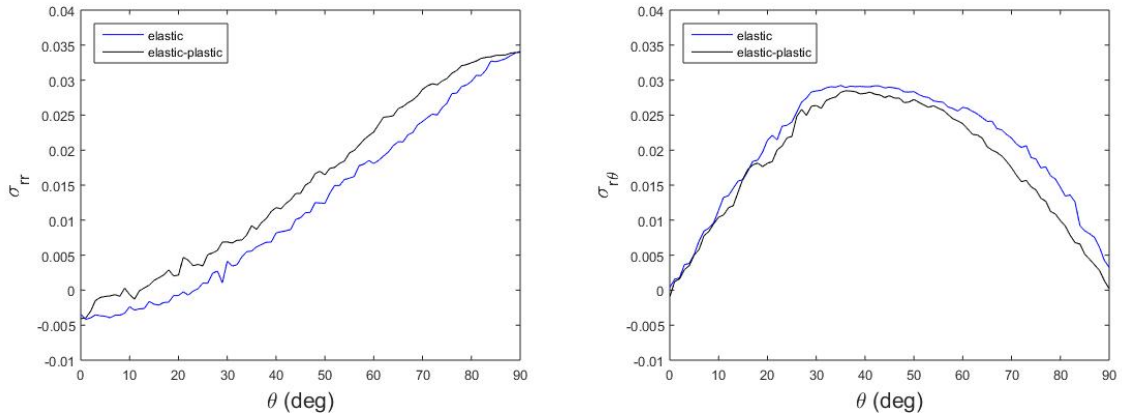

(a) Normal interfacial stress

(b) Tangent interfacial stress

Figure 5.4: Effect of plasticity on stress distribution around the fiber

For the system with an elastic fiber and matrix under transverse uniaxial tensile load, the maximum normal interfacial stress appears at the pole of the fiber. In Figure 5.4a, it can be seen that the maximum normal stress rather spreads over a region from $\theta = 80°$ to $\theta = 90°$ when the matrix follows elastic-plastic behavior law. For the tangent interfacial stress shown in Figure 5.4b, the maximum tangent interfacial stress occurs at roughly $\theta = 40°$ for both the case with elastic matrix and the case with elastic-plastic matrix. In Figure 5.4, it clearly shows that the interfacial stresses become lower when considering elastic-plastic matrix.

The effect of lateral boundary condition on stress distributions around the fiber is shown in Figure 5.5 when the fiber is embedded in an elastic-plastic matrix. The case with free lateral sides is denoted by BC type 1 while the case with fixed lateral sides is denoted by BC type 2.

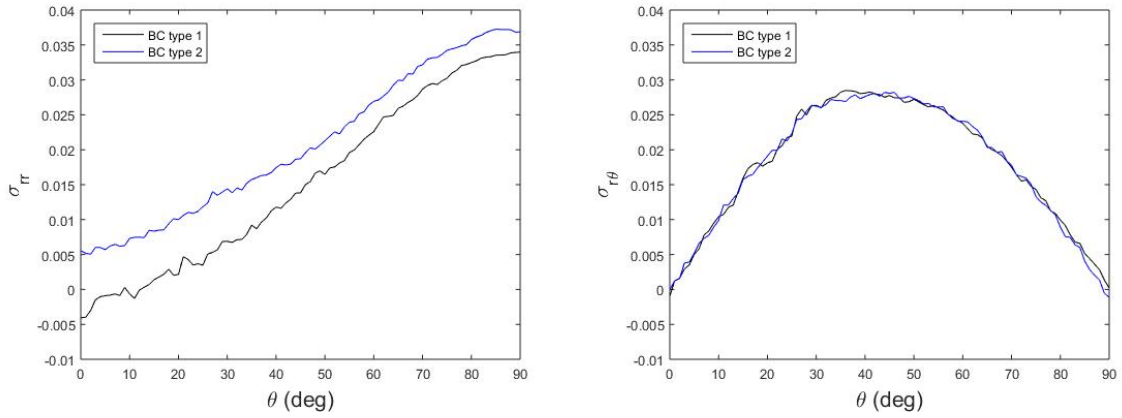

(a) Normal interfacial stress

(b) Tangent interfacial stress

Figure 5.5: Effect of boundary condition on stress distribution around the fiber

In Figure 5.5a, the radial stresses under the same prescribed displacement are compared. It can be seen that the interface is all under tension when the lateral sides are fixed while there is a small portion of the interface that the normal interfacial stresses are compressive and work against debonding when the lateral sides are free. This tensile stress perpendicular to the interface is one of the considerations of fiber debonding. It can also be seen that, when the lateral sides are fixed, the maximum normal interfacial stress is shifted a few degrees from the pole. However, the difference between the maximum stress and the stress at the pole is not significant.

For the tangent interfacial stress, it can be seen in Figure 5.5b that, under the same loading, different boundary conditions do not alter the distribution of tangent interfacial stress around the fiber.

5.3 Stress distribution along radial distance

Stress distributions along the radial distance are presented in this section. Since the fiber is usually much stiffer than the matrix, different level of stresses is developed because of this mismatch in material properties as seen in Figure 5.6. The stresses due to two different tensions are compared to show how the stresses evolve.

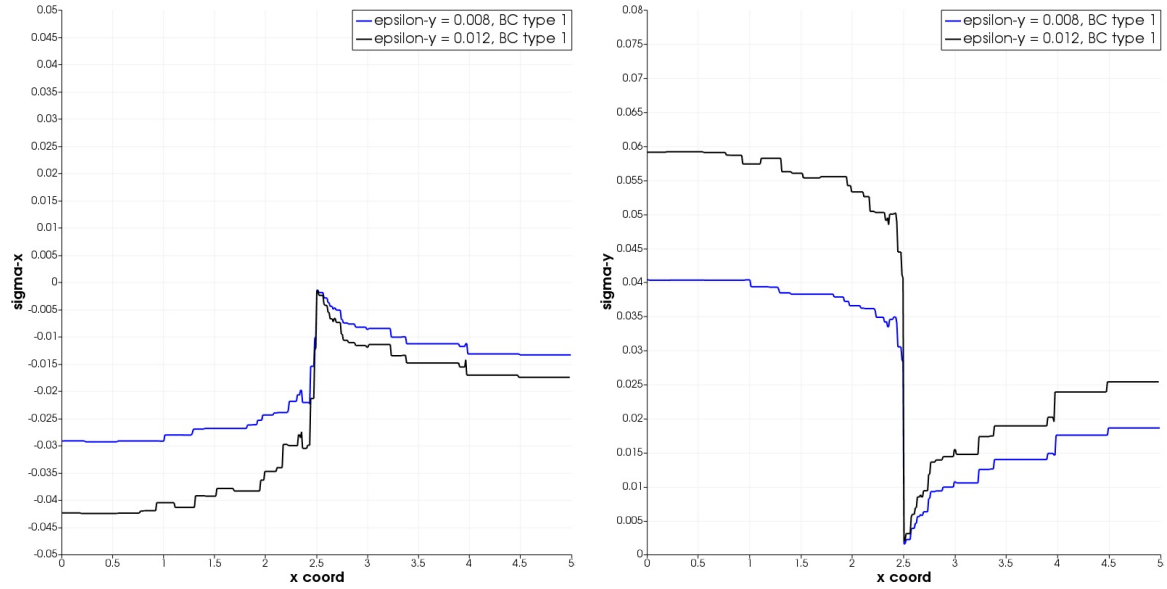

(a) Distribution of σ_x along x-axis

(b) Distribution of σ_y along x-axis

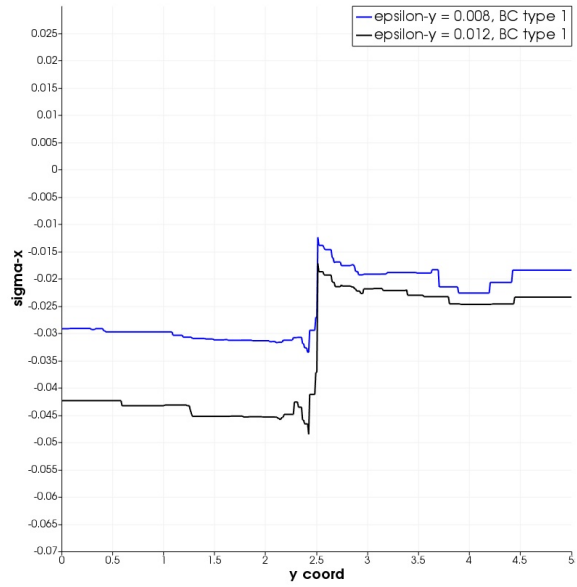

(c) Distribution of σ_x along y-axis

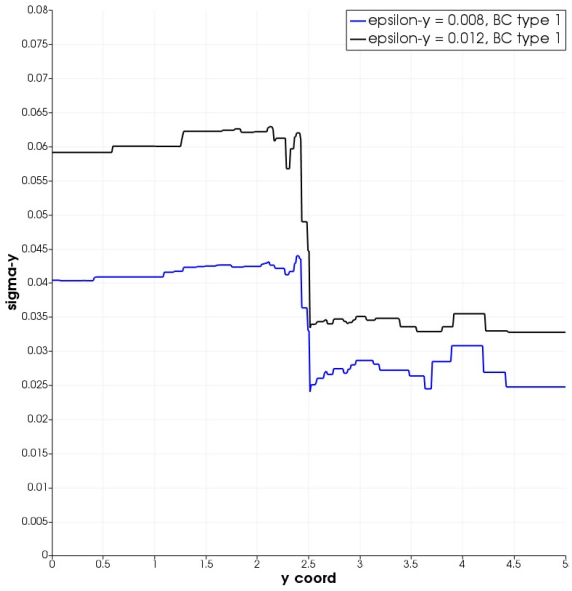

(d) Distribution of σ_y along y-axis

Figure 5.6: Stress distribution in the transverse and parallel direction to the tensile load

It can be seen in all plots in Figure 5.6 that all stresses are discontinuous at the interface. Stress magnitudes are at maximum in the fiber region and at minimum in the matrix at the fiber-matrix interface. Increase in the prescribed displacement results in larger difference at the interface. From Figure 5.6a and Figure 5.6c, stress σ_{xx} is compressive along both x-axis and y-axis. From Figure 5.6b and Figure 5.6d, stress σ_{yy} is tensile along both x-axis and y-axis and, from the minimum point, the stress σ_{yy} slowly increases and approaches the far-field value away from the interface in the matrix region.

The distribution of σ_{xx} along the x-axis is plotted in Figure 5.7 to show the effect of boundary conditions. It can be seen that, under the same prescribed displacement, the overall distributions are similar. For both types of boundary conditions, stress σ_{xx} is compressive in the fiber. However, the restriction in lateral sides causes tensile normal stress at the fiber-matrix interface. The stress decays as the radial coordinate increases and return to be compressive.

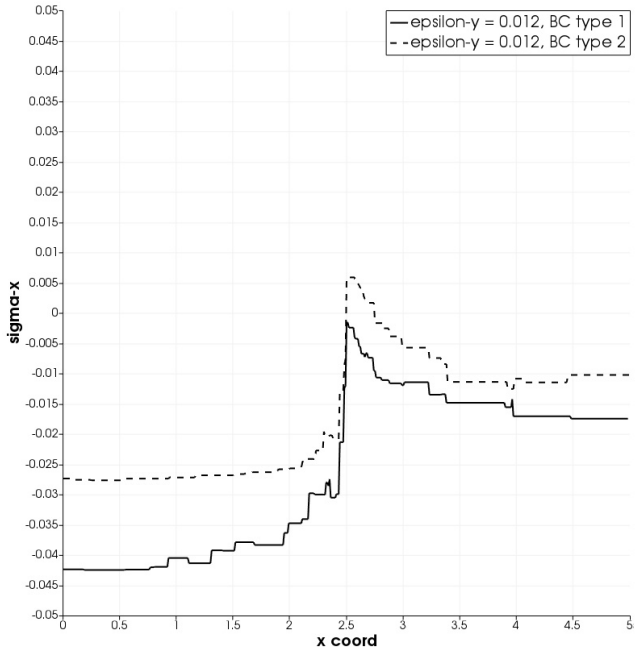

Figure 5.7: Effect of boundary condition on stress distribution along x-axis

The effect of plasticity on stress distribution in y-axis is shown in Figure 5.8. It can be seen that the stresses become lower when considering elastic-plastic matrix similar to what can be seen in the stress distribution around the fiber in the previous section.

Figure 5.9 shows the stress distribution along the radial distance due to shear load. Along x-axis, stress σ_{xy} increases gradually from the center of fiber, has its maximum value at the interface and gradually decay in the matrix region as seen in Figure 5.9a. Stress discontinuity is clearly seen along the diagonal radius ($\theta = 45°$ where the maximum macroscopic shear occurs as shown in Figure 5.9b.

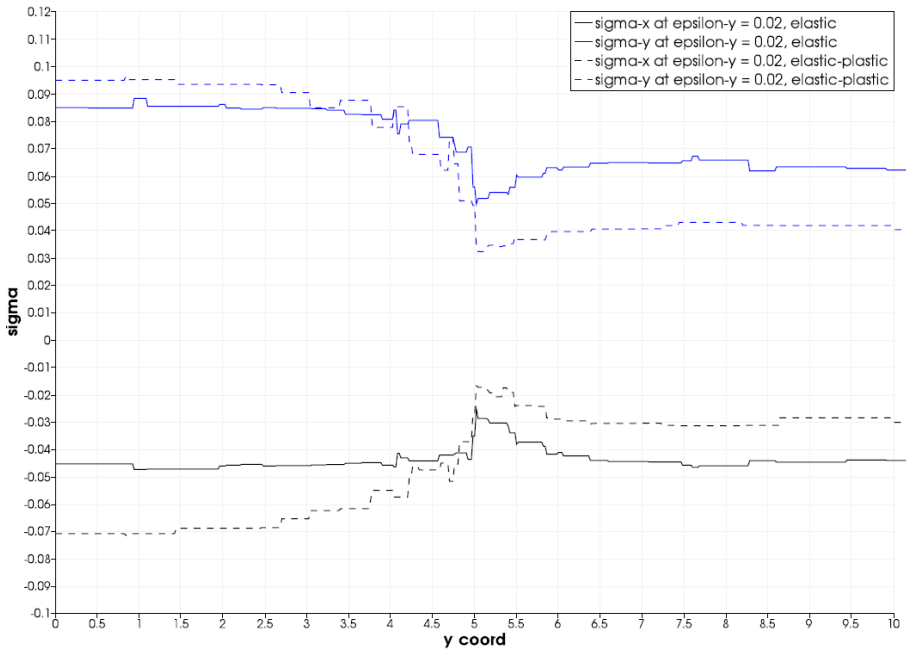

Figure 5.8: Effect of plasticity on stress distribution along y-axis

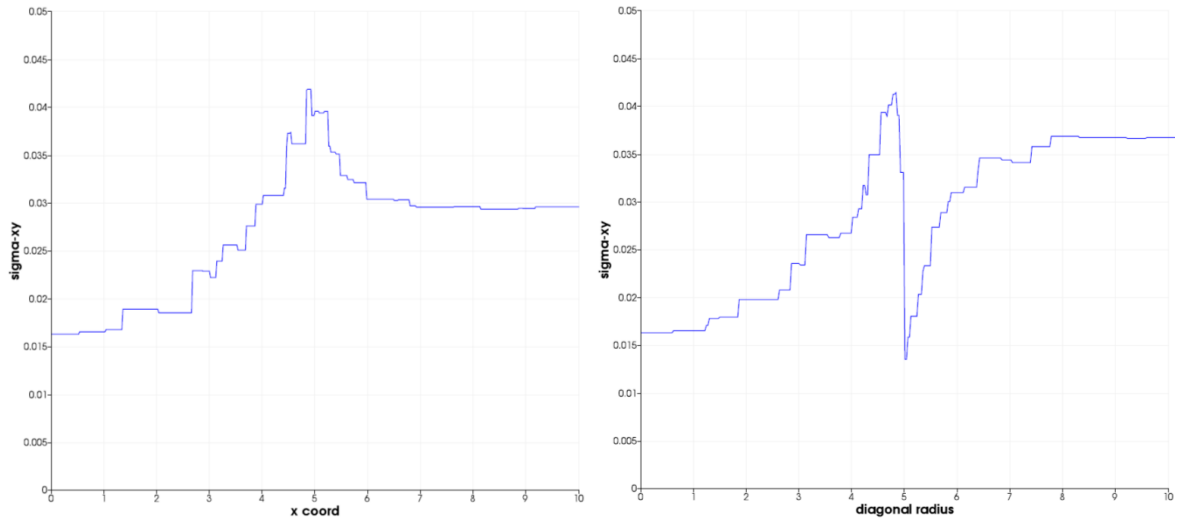

(a) Distribution of σ_{xy} along x-axis

(b) Distribution of σ_{xy} along 45° radius

Figure 5.9: Stress distribution in the radial distance due to shear

Chapter 6: Conclusions

The study of stress distribution in the vicinity of an elastic fiber embedded in a plastically deforming matrix was performed to validate the implementation of nonlinear constitutive law in CimLib. It is found that the overall results are in good agreement with the literature. The ability to include plastic matrix behavior in the analysis is helpful towards the determination of the local condition that could lead to damage mechanisms such as void nucleation or interfacial debonding.

The strong hypothesis of mixture law remains acceptable thanks to the relatively fine mesh at the interface though the discontinuity due to material properties will be better captured with finer mesh. The simulations experience costly computational time since the isotropic mesh adaptation still involves a large number of elements in the band around the interface even though the band is narrow compared to the size of the entire computational domain. Since CimLib is also capable of an anisotropic mesh adaptation, this approach could be useful.

Since the model considered is a simple configuration, it is possible to use a classical multi-domain finite element framework where the model is based on an explicit description of the matrix and fiber considering one mesh for each domain and contact conditions at the interface. However, the strategy used by CimLib is a part of a larger goal of modeling three phases consisting matrix, fiber and interlayer.

Bibliography

[1] Eshelby JD. The determination of the elastic field of an ellipsoidal inclusion and related problems. Proc Roy Soc A 1957; 241.

[2] Mori T, Tanaka K. Average stress in matrix and average elastic energy of materials with misfitting inclusions. Acta Metallurgica 1973; 21.

[3] Halpin JC, Kardos JL. The Halpin-Tsai equations: a review. Polymer Engineering and Science 1976; 16(5):344-352.

[4] Torquato S. Effective stiffness tensor of composite media: II. applications to isotropic dispersions. J Mech Phys Solids 1998; 46(8):1411-1440.

[5] Segurado J, Llorca J. A numerical approximation to the elastic properties of sphere-reinforced composites. J Mech Phys Solids 2002; 50:2107-2121.

[6] Liu H, Zeng D, Li Y, Jiang L. Development of RVE-embedded solid elements model for predicting effective elastic constants of discontinuous fiber reinforced composites. Mechanics of Materials 2016; 93:109-123.

[7] Segurado J, González C, Llorca J. A numerical investigation of the effect of particle clustering on the mechanical properties of composites. Acta Materialia 2003; 51:2355-2369.

[8] Tian W, Qi L, Zhou J, Liang J, Ma Y. Representative volume element for composites reinforced by spatially randomly distributed discontinuous fibers and its applications. Composite Structures 2015; 131:366-373.

[9] Huang H, Talreja R. Numerical simulation of matrix micro-cracking in short fiber reinforced polymer composites: initiation and propagation. Composites Science and Technology 2006; 66:2743-2757.

[10] Jiang X, Gao Q. Stress-transfer analysis for fibre/matrix interfaces in short-fibre-reinforced composites. Composites Science and Technology 2001; 61:1359-1366.

[11] Tandon GP, Weng GJ. Stress distribution in and around spheroidal inclusions and voids at finite concentration. J Appl Mech 1986; 53:511-518

[12] Orr J, Brown DK. Elasto-plastic solution for a cylindrical inclusion in plane strain. Engineering Fracture Mechanics 1974; 6:261-274.

[13] Wilner B. Stress analysis of particles in metals. J Mech Phys Solids 1988; 36(2):141-165.

[14] Lee BJ, Mear ME. Stress concentration induced by an elastic spheroidal particle in a plastically deforming solid. J Mech Phys Solids 1999; 47:1301-1336.

[15] Briottet L, Gilormini P, Montheillet F. Approximate analytical equations for the deformation of an inclusion in a viscoplastic matrix. Acta Mechanica 1999; 134:217-234.

[16] Ahmadi I, Aghdam MM. Elasto-plastic MLPG method for micromechanical modeling of heterogeneous materials. CMES 2015; 108(1):21-48.

[17] Schmid DW, Podladchikov YY. Analytical solutions for deformable elliptical inclusions in general shear. Geophys J Int 2003; 155:269-288.

[18] Pak YE, Mishra D, Yoo SH. Closed-form solution for a coated circular inclusion under uniaxial tension. Acta Mech 2012; 223:937-951.

[19] Voros G, Pukanszky B. Effect of a soft interlayer with changing properties on the stress distribution around inclusions and yielding of composites. Composites: Part A 2001; 343-352.

[20] Lauke B, Schuller T. Calculation of stress concentration caused by a coated particle in polymer matrix to determine adhesion strength at the interace. Composites Science and Technology 2002; 62:1965-1978.

[21] Sun Q, Meng Z, Zhou G, Lin SP, Kang H, Keten S, Guo H, Su X. Multi-scale computational analysis of unidirectional carbon fiber reinforced polymer composites under various loading conditions. Composites Structures 2018; 196:30-43.

[22] Silva L, Puaux G, Vincent M, Laure P. A monolithic finite element approach to compute permeabilityatc microscopic scales in LCM processes. 13th ESAFORM Conference on Material Forming, Brescia, Italy, April 2010; 3(Suppl.1):619-622.

[23] Hachem E, Kloczko T, Digonnet H, Coupez T. Stabilized finite element solution to handle complex heat and fluid flows in industrial furnaces using the immersed volume method. Int J Numer Meth Fluids 2012; 68:99-121.

[24] Roux E, Bernacki M, Bouchard P. A level-set and anisotropic adaptive remeshing strategy for the modeling of void growth under large plastic strain. Comput Mater Sci 2013; 68:32-46.

[25] Munoz DP, Bruchon J, Drapier S, Valdivieso F. A finite elemenet-based level set method for fluid-elastic solid interaction with surface tension. Int J Numec Meth Engng 2013; 93:919-941.

[26] Digonnet H, Silva L, Coupez T. CimLib: a fully parallel application for numerical simulations based on components assembly. AIP Conference Proceedings, volume 908, Porto, Portugal, 17-21 June 2007; 269.

[27] Shakoor M, Bernacki M, Bouchard PO. A new body-fitted immersed volume method for the modeling of ductile fracture at the microscale: analysis of void clusters and stress state effects on coalescense. Engineering Fracture Mechanics 2015; 147:398-417.